coatings

MDPI

Article

Gold Nanoparticles Decorated Titanium Oxide Nanotubes with Enhanced Antibacterial Activity Driven by Photocatalytic Memory Effect

Hongqin Zhu [1], Ji Tan [2], Jiajun Qiu [2], Donghui Wang [2,3], Zhe Zhao [1], Zihan Lu [1], Gaoshan Huang [1,*], Xuanyong Liu [2] and Yongfeng Mei [1]

[1] Department of Materials Science, State Key Laboratory of ASIC and System, Fudan University, Shanghai 200433, China
[2] State Key Laboratory of High Performance Ceramics and Superfine Microstructure, Shanghai Institute of Ceramics, Chinese Academy of Sciences, Shanghai 200050, China
[3] School of Health Sciences and Biomedical Engineering, Hebei University of Technology, Tianjin 300130, China
* Correspondence: gshuang@fudan.edu.cn

Abstract: Titanium and its alloys have been widely used for orthopedic and dental implants. However, implant failures often occur due to the implant-related bacterial infections. Herein, titanium oxide nanotubes (TNTs) with an average diameter of 75 nm were formed by anodizing on the surface of titanium, and subsequently gold (Au) nanoparticles were deposited on TNTs by magnetron sputtering (Au@TNTs). The antibacterial study shows that TNTs surface decorated with Au nanoparticles exhibits the preferable effect in restricting the growth of *Escherichia coli* (*E. coli*) and *Staphylococcus aureus* (*S. aureus*) even under dark conditions, and the antibacterial rates reached 84% and 75%, respectively. In addition, the constructed film showed no cytotoxicity. Such a selective bactericidal effect of Au@TNTs samples might be attributed to the photocatalytic memory effect, which provides a new insight in the designing of antibacterial surfaces for biomedical application.

Keywords: biomaterials; nanoparticles; porous materials; sputtering

Citation: Zhu, H.; Tan, J.; Qiu, J.; Wang, D.; Zhao, Z.; Lu, Z.; Huang, G.; Liu, X.; Mei, Y. Gold Nanoparticles Decorated Titanium Oxide Nanotubes with Enhanced Antibacterial Activity Driven by Photocatalytic Memory Effect. *Coatings* **2022**, *12*, 1351. https://doi.org/10.3390/coatings12091351

Academic Editor: Sara Ferraris

Received: 20 August 2022
Accepted: 14 September 2022
Published: 16 September 2022

1. Introduction

Titanium (Ti) and its alloys have been widely used for biomedical devices because of their outstanding mechanical properties [1] and excellent biocompatibility [2–4]. However, Ti-based implants lack bactericidal activities and are susceptible to bacterial infection [4,5]. Researchers have come up with numerous strategies to conquer bacterial infections. The most commonly used strategy is loading antibacterial agents on the implants [6,7]. However, it may cause drug resistance. Regulating the surface topography of implants is another widely investigated method, but it is only effective to bacteria adhering to the implant surface [8,9]. Recently, a series of stimuli-responsive implants have been developed, which can combat bacterial infection by coupling with external stimuli such as light, ultrasound, etc. [10,11]. However, the application of stimuli-responsive implants is limited by the penetration depth of the external field to the human body. Moreover, exposure to various external fields for a long time may cause damage to the human tissue, increasing the safety concerns. How to endow Ti-based implants with preferable bactericidal activity without scarifying their biocompatibility remains a great challenge.

During the last decade, titanium dioxide nanotubes (TNTs) have attracted extensive attention in different research fields due to their great cytocompatibility [12,13], osseointegration [14,15], and photocatalytic activity [16]. Under light irradiation, TNTs produce electron-hole pairs which can promote the generation of reactive oxygen species (ROS), thus killing bacteria with high efficiency [17]. However, TNTs exhibit no antibacterial

ability in dark, limiting their in vivo application. Recent studies have indicated that some semiconductor materials (such as CuO, WO_3, SnO_2, CuSe, etc.) have capacitive characteristics, which can store photogenerated electrons [18–21]. The combination of these semiconductors with TiO_2 induces a photocatalytic memory effect, which can produce ROS and inhibit the growth of bacteria in dark [22–24]. Unfortunately, most of the semiconducting compounds contain elements with a low cellular tolerance such as Cu and Se, raising the biosafety concern [25]. Therefore, using biosafety nanomaterials to construct a platform for electron storing under light irradiation and electron release to kill bacteria under dark conditions is a promising strategy to modify the Ti-based implant to avoid bacterial infection.

Gold in bulk is highly unreactive and chemically inert by nature, thus exhibiting good biocompatibility. In addition, its nanosized particles (Au NPs) have various excellent properties (such as photocatalysis and photothermal) and are exploited for diverse applications (such as electrochemistry, environmental engineering, and biomedicine) [26–28]. Meanwhile, for the biomedical applications, the biosafety of Au NPs attracts great attention. In in vivo studies, it is found that Au NPs have side effects in hematology, blood chemistry, and in the inflammatory and pathological response [29–32]. Nevertheless, the toxicity of Au NPs is detected via intraperitoneal injection. When Au NPs are deposited on implant surface, the adhesion strength is rather strong. Furthermore, considering the limited amount of Au ions released from the Au NPs, it is predictable that Au NPs fabricated on implants surface have superior biocompatibility. On the other hand, previous studies have revealed that gold metallization on the implant surface is able to increase the charge separation, thus facilitating the photocatalytic process [33,34], For instance, Wang et al. immobilized Au NPs on titanium dioxide nanoparticles for the photocatalytic evolution of hydrogen [35]. Therefore, the deposition of Au NPs on TNTs has been considered as a desirable approach to store electrons for antibacterial application with good biosafety.

Herein, Au NPs with good capacitive property are chosen to be integrated with TNTs (Au@TNTs) in order to improve the antibacterial performance of a Ti implant without affecting its biocompatibility. Electrons in the valence band of TNTs located at a higher energy level can be injected and stored in Au NPs under light irradiation, and they continuously release charges in dark, which can eradicate bacterial infection. It is found that, even under dark conditions, the constructed films exhibited excellent antibacterial ability and present no toxic effects to cells. Our study may provide new insight into the design of antibacterial implants.

2. Materials and Methods

2.1. Sample Preparation

Figure 1 illustrates the process to construct the Au NPs-decorated TNTs on Ti. Briefly, commercially pure Ti plates (10 mm × 10 mm × 1 mm; Grade TA3, 99.98% purity) were ultrasonically washed and denoted as Ti. Then, TNTs were formed on the Ti surface by electrochemical anodization in 1.0 wt.% hydrofluoric acid aqueous solution at 20 V for 30 min via a DC power supply (Model 62024P-600-8) [36]. After anodization, the samples were annealed at 450 °C for 2 h and named as TNTs. Au NPs were sputtered on both Ti and TNTs samples with a sputtering current of 20 mA for 120 s using an ion sputter instrument (E-1045, Hitachi, Tokyo, Japan), and the resultant samples were named as Au@Ti and Au@TNTs, respectively.

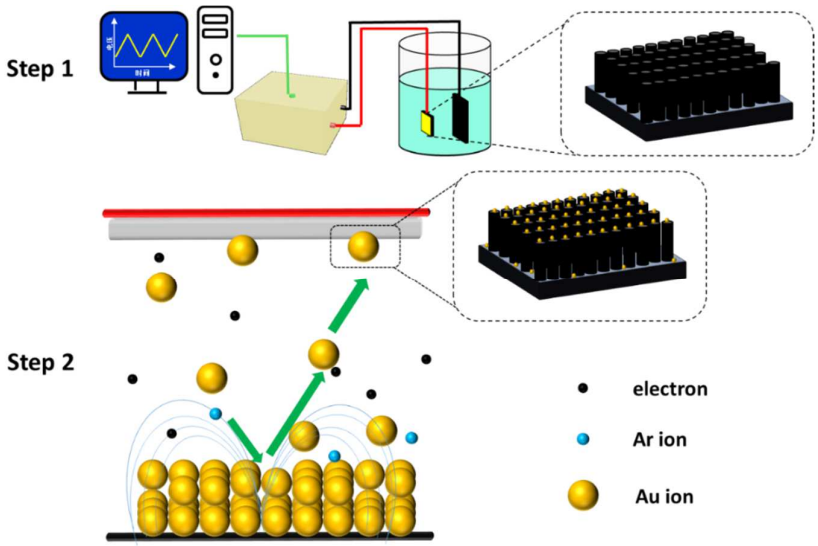

Figure 1. Schematic diagrams of the process to construct Au@TNTs.

2.2. Surface Characterization

The samples were characterized by scanning electron microscopy (SEM, SU 8220, Hitachi, Tokyo, Japan), energy dispersive spectroscopy (EDS, X-MaxN, Oxford, UK), X-ray photoelectron spectroscopy (XPS, PHI5300, PerkinElmer, Boston, MA, USA), and X-ray diffraction (XRD, D2 PHASER, Bruker, Karlsruhe, Germany). Tafel curves of the samples were measured by CHI 760C electrochemical workstation in normal saline. Photocurrent measurements were performed by an electrochemical analyzer (CHI66D, Shanghai Chenhua Instruments Co., Ltd., Shanghai, China).

2.3. Antibacterial Property Assessment

E. coli (ATCC 25922, Institute of Microbiology, Chinese Academy of Sciences, Beijing, China) and *S. aureus* (ATCC 25923, Institute of Microbiology, Chinese Academy of Sciences, Beijing, China) were used to evaluate the antibacterial activity. A total of 60 uL of bacterial suspension (10^7 CFU/mL) was seeded and cultured at 37 °C for 24 h. Then, the bacteria were fixed and observed by SEM. For plate colony counting, bacteria on the samples were collected, culturing for 24 h. A total of 100 uL of diluted bacterial suspension was introduced onto agar culture plates and cultured for another 18 h. Finally, images of agar culture plates were obtained. The activity of bacteria was determined using an alamarBlue® assay after culturing for 12 h.

2.4. Cytocompatibility Assessment

The rat bone marrow mesenchymal stem cells (rBMSCs, Stem Cell Bank, Chinese Academy of Sciences, Shanghai, China) were used to evaluate the cytocompatibility of various samples. The rBMSCs (5×10^4 cells/mL) were inoculated on the surface of the samples and cultured for 12, 24 and 48 h. Thereafter, 500 µL of mixed live/dead cell-staining reagent (Biovaision, Waltham, MA, USA) was used to stain the cells. After rinsing with PBS (Aladdin, Shanghai, China), the cells were observed using fluorescence microscopy.

2.5. Statistical Analysis

At least three replicates were detected for each quantitative experiment. Results were presented as mean ± standard deviation (SD). GraphPad Prism 8 statistical software package was used to conduct statistical analyses. Statistically significant differences (p) were analyzed by unpaired t-test, one-way analysis of variance (ANOVA), two-way ANOVA, and Tukey's multiple comparison tests. * $p < 0.05$. ** $p < 0.01$. *** $p < 0.001$. **** $p < 0.0001$.

3. Results

Surface morphologies of Ti, TNTs, Au@Ti, and Au@TNTs are presented in Figure 2a. It is indicated that Ti exhibits a flat surface and TNTs samples are covered by ordered TiO_2 nanotubes. The average tube diameter of TNTs was 75 ± 15 nm (Figure 2b), the wall-thickness was 12 ± 2 nm (Figure 2c). Au NPs with uniform distribution can be observed on Au@Ti and Au@TNTs, and the average diameter of Au NPs was 23 ± 3 nm (Figure 2d). Moreover, the structure of TNTs is preserved after the decoration of Au NPs. EDS results shown in Figure 2e and Table 1 indicate that Au signals are only detected on Au@Ti and Au@TNTs, while absent on Ti and TNTs. EDS data are also confirmed by XPS measurements (Figure 2f) that Ti and TNTs samples only contain Ti, C, and O elements. The surface of Ti would be oxidized naturally, so O element was also detected in Ti group. In comparison, the additional peaks corresponding to Au 4d and Au 4f are observed from Au@Ti and Au@TNTs samples. Furthermore, the high-resolution spectra (Figure 2g) suggest that the deposited Au NPs are in zero-valence state, which validates that the elemental Au NPs have been successfully deposited [37]. XRD patterns (Figure 2h) show that only metal Ti phases appear on Ti and Au@Ti samples. However, the addition XRD peaks corresponding to TiO_2 phase emerge on the TNTs and Au@TNTs samples [38].

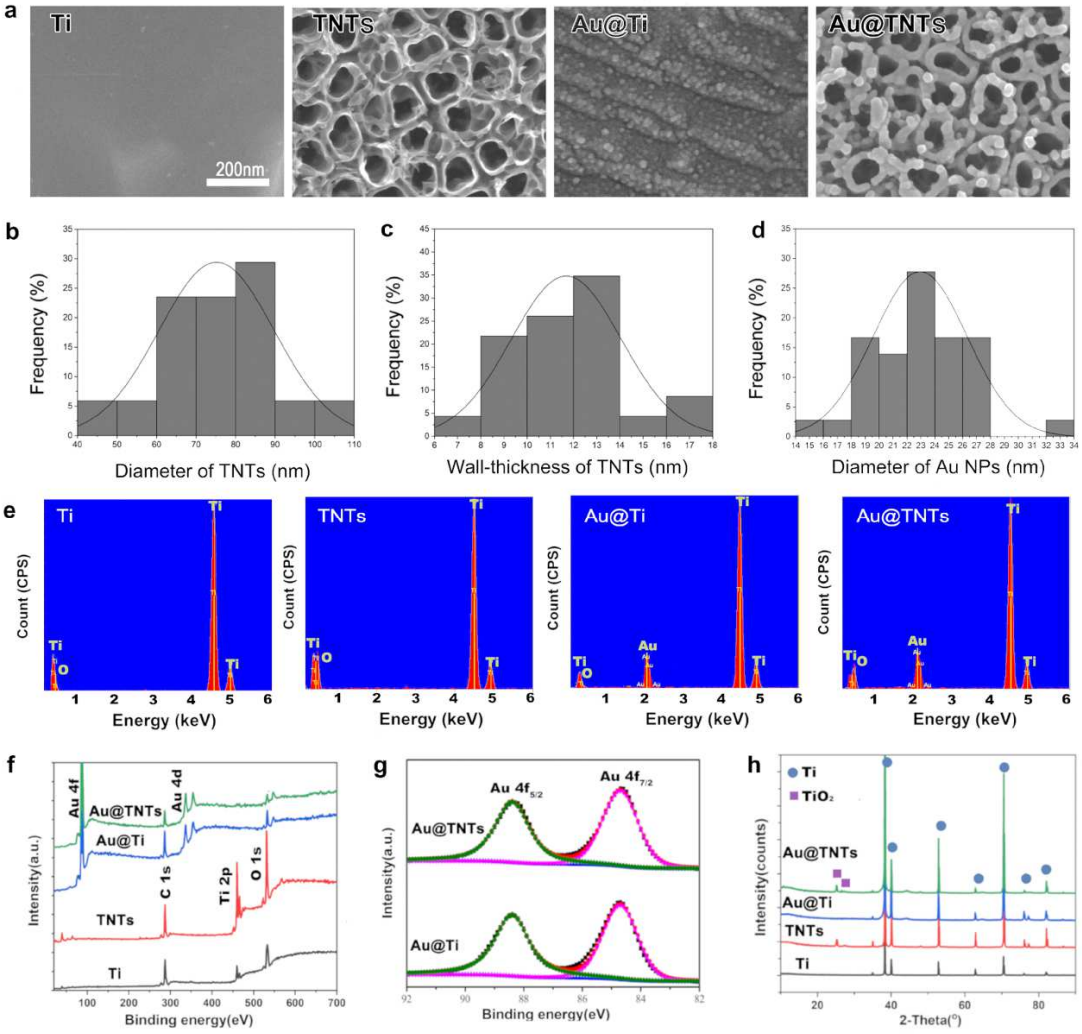

Figure 2. (**a**) SEM images of Ti, TNTs, Au@Ti and Au@TNTs samples. (**b**) Diameter distribution of TNTs. (**c**) Wall-thickness distribution of TNTs. (**d**) Diameter distribution of Au NPs on Au@TNTs sample. (**e**) EDS and (**f**) XPS spectra of Ti, TNTs, Au@Ti, and Au@TNTs samples. (**g**) High-resolution XPS spectra of Au for Au@Ti and Au@TNTs samples. (**h**) XRD spectra of various samples.

Table 1. Chemical composition of different samples.

-	Ti (at.%)	TNTs (at.%)	Au@Ti (at.%)	Au@TNTs (at.%)
Ti	81.7	37.0	83.8	56.1
O	18.3	63.0	14.8	42.3
Au	-	-	1.4	1.6

E. coli and *S. aureus* were cultured on four different samples in dark conditions to mimic the in vivo environment. SEM was utilized to monitor the morphologies of *E. coli* and *S. aureus* (Figure 3a). Both *E. coli* and *S. aureus* are well grown on surface of the Ti, TNTs, and Au@Ti samples, obvious filamentous pseudopodia can be observed. However, bacterial membranes are remarkably shrunken on Au@TNTs samples and the bacterial numbers are reduced considerably. The agar plate images (Figure 3b) show that the colony numbers of *E. coli* and *S. aureus* are quite similar in Ti, TNTs, and Au@Ti groups, but dramatically decreased in Au@TNTs group. The bacterial viability is further evaluated by fluorescence measurements (Figure 3c), and the results also suggest that the activity of bacteria cultured on Au@TNTs samples has been suppressed effectively.

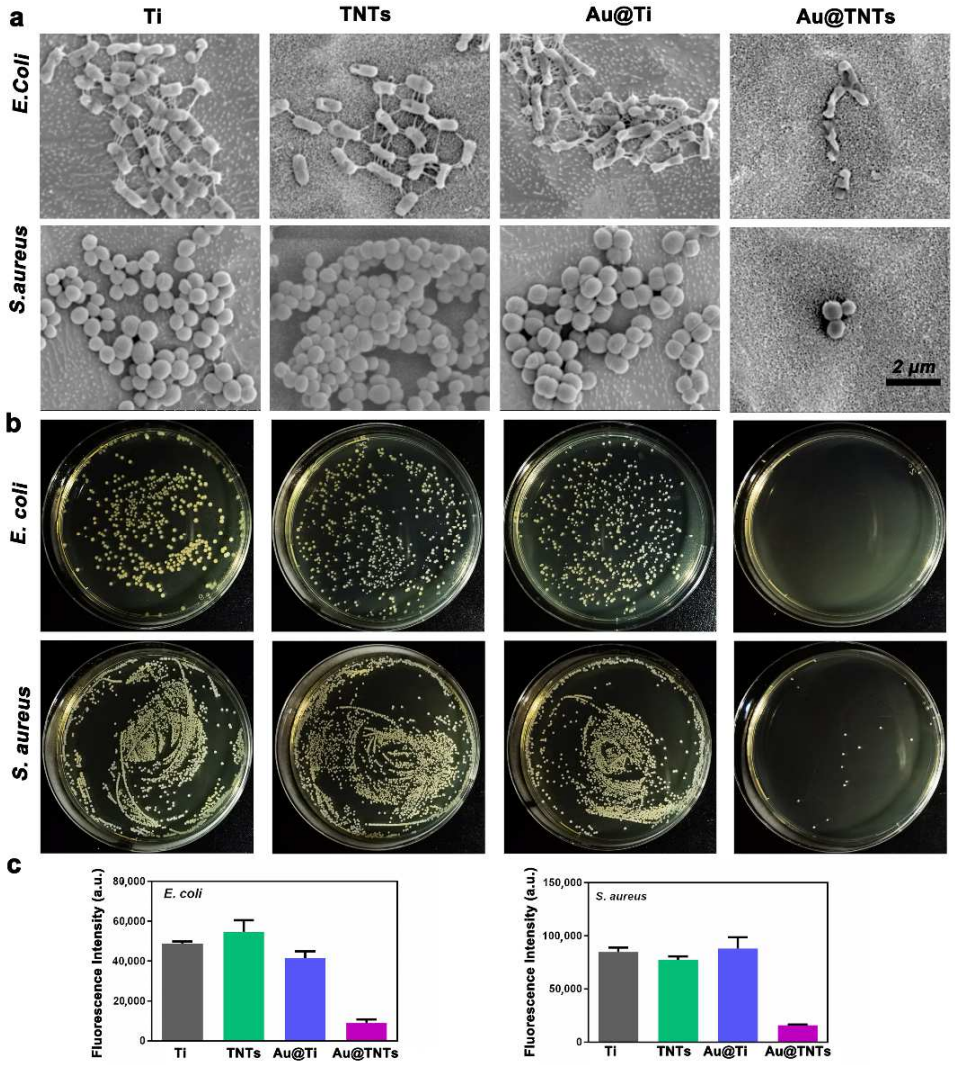

Figure 3. SEM images of *E. coli* and *S. aureus* grown on different samples (**a**). Typical photographs of *E. coli* and *S. aureus* cultured on nutrient broth medium agar for 18 h (**b**). Viability of *E. coli* and *S. aureus* evaluated by fluorescence measurements (**c**).

The viability of mesenchymal stem cells is a determining factor for the successful implantation. rBMSCs have become the predominant cells used to assess the osteogenic function and cytotoxicity of the hard tissue implant. Therefore, in this study, the biocompatibility of the prepared samples was tested by culturing rBMSCs on the sample surface, and the cells were stained by a live/dead staining kit. After culturing for 12 and 24 h, no obvious differences could be detected on the live/dead states of cells cultured on various samples (Figure 4a,b). Most cells on Au@TNTs were alive (stained green) and dead cells (stained red) could be barely observed. After 48 h of cultivation, more live cells appeared on Au@TNTs than other samples (Figure 4b), revealing their satisfactory cytocompatibility.

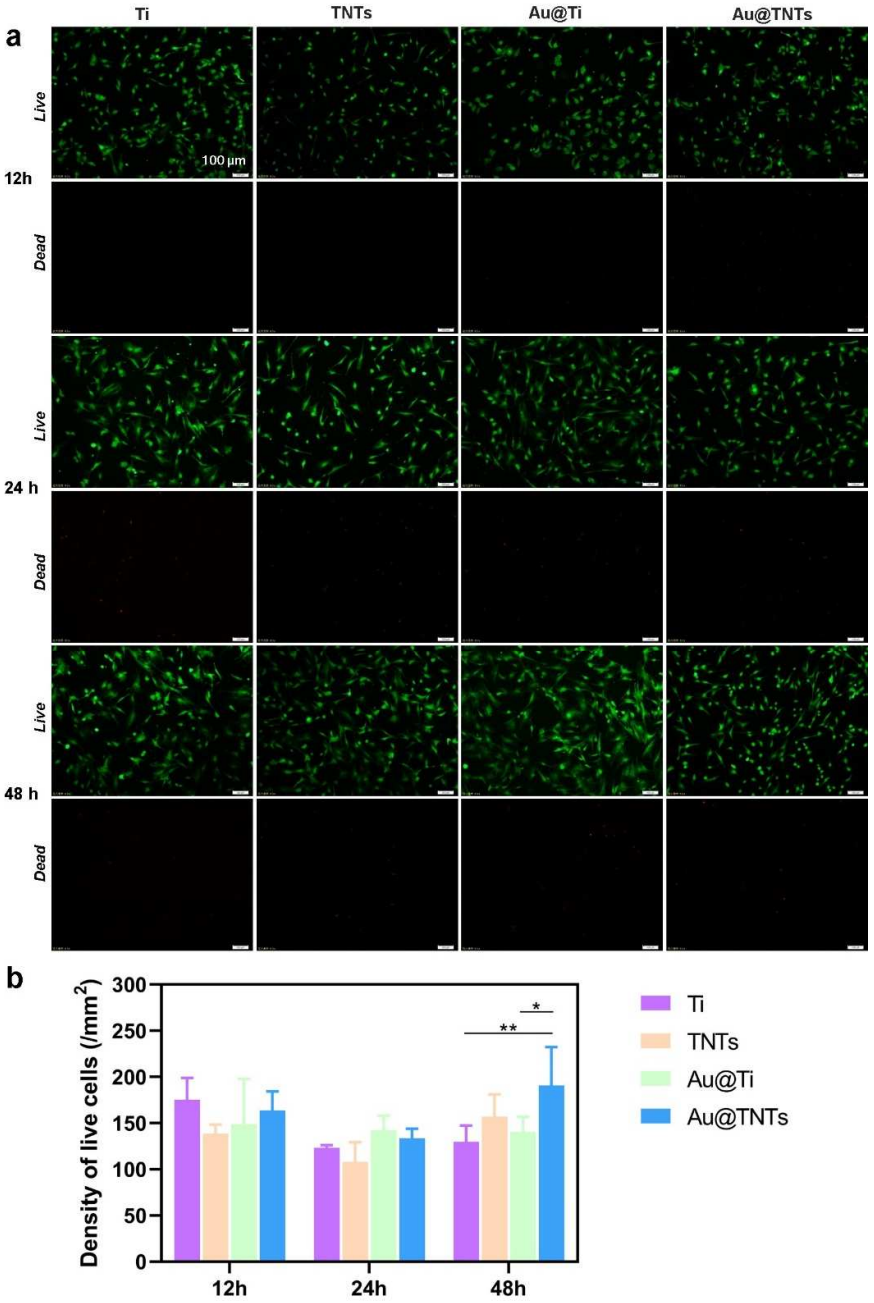

Figure 4. (**a**) Fluoroscopy images of live/dead staining of rBMSCs cells on various samples. (**b**) Density of live cells after 12, 24, and 48 h of culture on different samples ($n = 6$, * $p < 0.05$, ** $p < 0.01$).

4. Discussions

It is considered that the dark condition is similar to the in vivo environment, meaning that the enhanced antibacterial activity of Au@TNTs samples might stem from the photocatalytic memory effect due to their unique heterogeneous structures (Figure 5a). Under light irradiation, the electrons in the valence band of titanium dioxide might be excited and transited to the conduction band, leaving holes in the valence band. Both electrons and holes can react with substances in the environment to form ROS and play an antibacterial role [39]. Moreover, once the light irradiation is switched off, the electrons and holes recombine and annihilate quickly, which results in the vanishing of the antibacterial ability of TNTs in the dark environment. However, the situation changes dramatically as TNTs are decorated with Au NPs to form Au@TNTs. The conduction band of TNTs is at −4.14 eV and the Fermi energy level of Au NPs is at −5.1 eV. When TNTs and Au NPs are in contact, some electrons in the valence band of TNTs located at a higher energy level can be injected and stored in Au NPs owning to their capacitive characteristics. In dark environment, the electrons stored in Au NPs are gradually released into the environment and further react with oxygen to produce O_2^- radicals, which causes the rupture of the bacterial membrane, and ultimately leads to bacterial death. The above hypothesis can be verified by the Tafel and photocurrent curve measurements. The Tafel polarization curves (Figure 5b) indicate that Ti, TNTs, and Au@Ti exhibit similar exchange current density, while the current density of Au@TNTs is one order of magnitude higher, which is ascribed to the enhanced charge transfer of Au@TNTs affected by electrons stored in the Au NPs. The photo-response of different samples is shown in Figure 5c. Without the integration of TNTs, no continuous and stable photocurrent is obtained on Ti and Au@Ti samples. However, the considerable photocurrents are generated in TNTs and Au@TNTs samples. In particular, negative net photocurrent can be observed from Au@TNTs samples, verifying the capacitive behavior of Au NPs decorated on TNTs, which can store electrons under light illumination and release electrons in dark condition. In fact, the photocatalytic memory effect is frequently observed in TiO_2 decorated by materials with capacitive characteristics, in which the antibacterial ability is significant improved due to the formation of unique heterogeneous structures [22,40–42]. Li et al. decorated a nitrogen-doped titanium oxide (TiON) matrix with palladium oxide (PdO) nanoparticles, and the optoelectronic coupling between PdO and TiON introduces a unique catalytic memory effect on bacterial disinfection due to the discharging of trapped electrons on PdO nanoparticles in the dark [40]. Liu et al. constructed a novel Cu_2O/TiO_2 composite, which showed a post-illumination bacteria disinfection effect [43]. Li et al. designed a Ag-modified TiO_2 film, which produced a synergistic antifungal mechanism under both light and dark conditions [44]. In this work the photocatalytic memory effect in Au@TNTs also occurs in dark condition and enables the improvement of antibacterial ability, which is essential for the initial period of implant surgery. In addition, no cytotoxic elements are introduced in the platform, thus eliminating the biosafety concerns. It should be noted that the constructed platform possesses antibacterial activity for certain period since the number of the stored electrons is limited. However, the improved antibacterial capability with certain period is sufficient for its clinical applicability since the demand for antibacterial property of implanted devices is time dependent. Bacterial infection is most likely to occur within the first few days after surgery [45,46]. Thereafter, the host immune system could be stimulated and reduce the infection risk considerably. However, the implant material can still be disturbed by bacteria in long-term applications, and foreign body reactions can cause the body to reject the implant and create a fibrous layer. Furthermore, it is a relatively expensive surface modification method owning to the usage of gold.

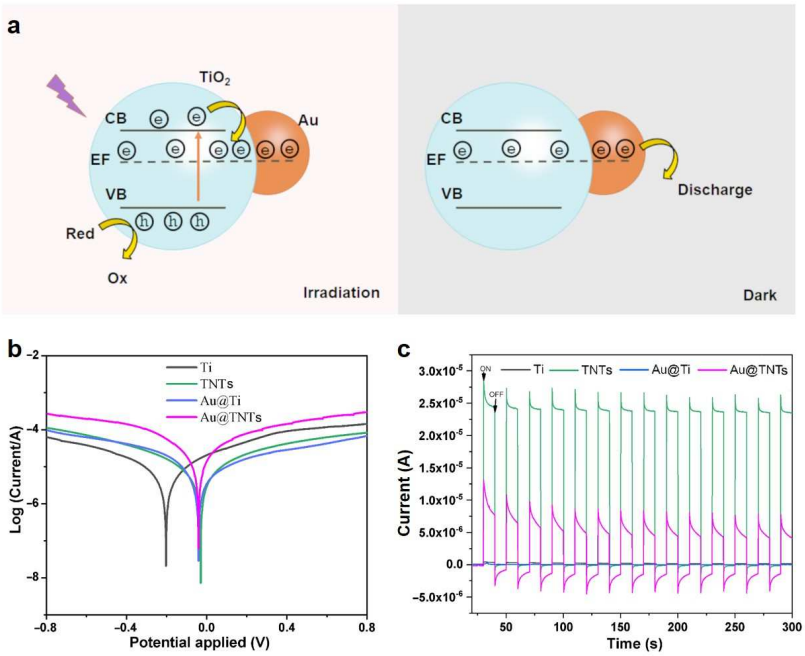

Figure 5. Schematic diagram for the photocatalytic memory effect of Au@TNTs samples (**a**). Tafel curves (**b**) and photocurrent curves (**c**) of various samples.

5. Conclusions

In summary, Au NPs-decorated TNTs exhibit superior antibacterial activities against *S. aureus* and *E. coli* without inducing obvious cytotoxicity. Due to the capacitive characteristics of Au NPs, the stored electrons are released in dark conditions. The released electrons react with oxygen to produce O_2^- radicals, which can destroy the bacterial membrane, thus yielding the antibacterial effect. It is expected that the integration of Au@TNTs can sufficiently suppress the growth of bacteria, which can improve the anti-bacterial performance of Ti based implants. However, it should be emphasized that there is more work that needs to be done before the clinical application of Au@TNTs, which includes prolonging the in vivo antibacterial time and improving economical and biocompatibility of the platform. Future studies should focus on bone integration of the TNTs and its compatibility with bone tissues, which might be achieved through other safer and cheaper metal nanoparticles combined with TNTs. In addition to the selection of metal particles, other aspects considering the textured surface, geometric parameters, and coating application also need to be carried out in the future to minimize implant failures.

Author Contributions: Conceptualization, H.Z.; methodology, J.T., J.Q. and D.W.; software, H.Z.; validation, H.Z., D.W. and X.L.; formal analysis, J.T. and D.W.; investigation, H.Z.; resources, Z.Z.; data curation, H.Z. and J.Q.; writing—original draft preparation, H.Z. and D.W.; Writing—review and editing, G.H., Y.M. and Z.L.; supervision, G.H. and Y.M.; funding acquisition, X.L., G.H. and Y.M. All authors have read and agreed to the published version of the manuscript.

Funding: The work was supported by the National Natural Science Foundation of China (Nos. 51961145108 and 51831011) and the Science and Technology Commission of Shanghai Municipality (No. 22ZR1405000).

Institution Review Board Statement:: Not applicable.

Informed Consent Statement: Not applicable.

Data Availability Statement: The authors confirm that the data supporting the findings of this study are available within the article.

Conflicts of Interest: The authors declare that they have no known competing financial interests or personal relationships that could have appeared to influence the work reported in this paper.

References

1. Jamari, J.; Ammarullah, M.I.; Santoso, G.; Sugiharto, S.; Supriyono, T.; van der Heide, E. In silico contact pressure of metal-on-metal total hip implant with different materials subjected to gait loading. *Metals* **2022**, *12*, 1241. [CrossRef]
2. Liu, X.; Chu, P.; Ding, C. Surface modification of titanium, titanium alloys, and related materials for biomedical applications. *Mater. Sci. Eng. R Rep.* **2004**, *47*, 49–121. [CrossRef]
3. Asadi, S.; Mortezagholi, B.; Hadizadeh, A.; Borisov, V.; Ansari, M.J.; Majdi, H.S.; Nishonova, A.; Adelnia, H.; Far, B.F.; Chaiyasut, C. Ciprofloxacin-loaded titanium nanotubes coated with chitosan: A promising formulation with sustained release and enhanced antibacterial properties. *Pharmaceutics* **2022**, *14*, 1359. [CrossRef] [PubMed]
4. Tong, S.; Sun, X.; Wu, A.; Guo, S.; Zhang, H. Improved biocompatibility of TiO_2 nanotubes via co-precipitation loading with hydroxyapatite and gentamicin. *Coatings* **2021**, *11*, 1191. [CrossRef]
5. Vacca, C.; Contu, M.P.; Rossi, C.; Ferrando, M.L.; Blus, C.; Szmukler-Moncler, S.; Scano, A.; Orru, G. In vitro interactions between streptococcus intermedius and streptococcus salivarius k12 on a titanium cylindrical surface. *Pathogens* **2020**, *9*, 1069. [CrossRef]
6. Jin, G.; Qin, H.; Cao, H.; Qian, S.; Zhao, Y.; Peng, X.; Zhang, X.; Liu, X.; Chu, P.K. Synergistic effects of dual Zn/Ag ion implantation in osteogenic activity and antibacterial ability of titanium. *Biomaterials* **2014**, *35*, 7699–7713. [CrossRef]
7. Jin, G.; Qin, H.; Cao, H.; Qiao, Y.; Zhao, Y.; Peng, X.; Zhang, X.; Liu, X.; Chu, P.K. Zn/ag micro-galvanic couples formed on titanium and osseointegration effects in the presence of s-aureus. *Biomaterials* **2015**, *65*, 22–31. [CrossRef]
8. Ghimire, A.; Song, J. Anti-periprosthetic infection strategies: From implant surface topographical engineering to smart drug-releasing coatings. *ACS Appl. Mater. Interfaces* **2021**, *13*, 20921–20937. [CrossRef] [PubMed]
9. Le Clainche, T.; Linklater, D.; Wong, S.; Phuc, L.; Juodkazis, S.; Le Guevel, X.; Coll, J.-L.; Ivanova, E.P.; Martel-Frachet, V. Mechano-bactericidal titanium surfaces for bone tissue engineering. *ACS Appl. Mater. Interfaces* **2020**, *12*, 48272–48283. [CrossRef]
10. Yuan, Z.; Tao, B.; He, Y.; Mu, C.; Liu, G.; Zhang, J.; Liao, Q.; Liu, P.; Cai, K. Remote eradication of biofilm on titanium implant via near-infrared light triggered photothermal/photodynamic therapy strategy. *Biomaterials* **2019**, *223*, 119479. [CrossRef]
11. Li, M.; Li, L.; Su, K.; Liu, X.; Zhang, T.; Liang, Y.; Jing, D.; Yang, X.; Zheng, D.; Cui, Z.; et al. Highly effective and noninvasive near-infrared eradication of a staphylococcus aureus biofilm on implants by a photoresponsive coating within 20 min. *Adv. Sci.* **2019**, *6*, 1900599. [CrossRef] [PubMed]
12. Wang, Y.; Wen, C.; Hodgson, P.; Li, Y. Biocompatibility of TiO_2 nanotubes with different topographies. *J. Biomed. Mater. Res. Part A* **2014**, *102*, 743–751. [CrossRef]
13. Coman, A.N.; Mare, A.; Tanase, C.; Bud, E.; Rusu, A. Silver-deposited nanoparticles on the titanium nanotubes surface as a promising antibacterial material into implants. *Metals* **2021**, *11*, 92. [CrossRef]
14. Liang, X.; Chen, L.; Lu, J.; Gao, X.; Chai, H. Preparation of titanium dioxide nanotube-based dental implants for osteogenesis and osseointegration acceleration. *Sci. Adv. Mater.* **2021**, *13*, 1195–1204. [CrossRef]
15. Feng, W.; Liu, N.; Gao, L.; Zhou, Q.; Yu, L.; Ye, X.; Huo, J.; Huang, X.; Li, P.; Huang, W. Rapid inactivation of multidrug-resistant bacteria and enhancement of osteoinduction via titania nanotubes grafted with polyguanidines. *J. Mater. Sci. Technol.* **2021**, *69*, 188–199. [CrossRef]
16. Abela, S.; Farrugia, C.; Xuereb, R.; Lia, F.; Zammit, E.; Rizzo, A.; Refalo, P.; Grech, M. Photocatalytic activity of titanium dioxide nanotubes following long-term aging. *Nanomaterials* **2021**, *11*, 2823. [CrossRef]
17. Yamaguchi, M.; Abe, H.; Ma, T.; Tadaki, D.; Hirano-Iwata, A.; Kanetaka, H.; Watanabe, Y.; Niwano, M. Bactericidal activity of tio2 nanotube thin films on si by photocatalytic generation of active oxygen species. *Langmuir* **2020**, *36*, 12668–12677. [CrossRef]
18. Cho, E.-C.; Chang-Jian, C.-W.; Huang, J.-H.; Huang, T.-Y.; Wu, N.-J.; Li, M.-T.; Chen, Y.-L.; Hsu, S.-C.; Weng, H.C.; Lee, K.-C. Preparation of $Ni(OH)_2$/CuO heterostructures for improved photocatalytic degradation of organic pollutants and microorganism. *Chemosphere* **2022**, *300*, 134484. [CrossRef]
19. Zhu, B.; Hong, X.; Tang, L.; Liu, Q.; Tang, H. Enhanced photocatalytic CO_2 reduction over 2D/1D $BiOBr_{0.5}Cl_{0.5}/WO_3$ S-scheme heterostructure. *Acta Phys. Chim. Sin.* **2022**, *38*, 2111008.
20. Zhao, L.; Li, G.; Li, F.; Yao, M. Enhanced visible light photoactivity of TiO_2/SnO_2 films by tridoping with Y/F/Ag ions. *J. Rare Earths* **2022**, *40*, 616–625. [CrossRef]
21. Chen, H.; Xing, Y.; Liu, S.; Fu, J.; Shi, H.; Liang, Y.; Wang, L.; Wang, W. Efficient pollutant degradation under ultraviolet to near-infrared light irradiation and dark condition using cuse nanosheets: Mechanistic insight into degradation. *J. Colloid Interface Sci.* **2022**, *613*, 103–116. [CrossRef]
22. Cai, T.; Liu, Y.; Wang, L.; Zhang, S.; Ma, J.; Dong, W.; Zeng, Y.; Yuan, J.; Liu, C.; Luo, S. "Dark deposition" of ag nanoparticles on TiO_2: Improvement of electron storage capacity to boost "memory catalysis" activity. *ACS Appl. Mater. Interfaces* **2018**, *10*, 25350–25359. [CrossRef] [PubMed]
23. Ezati, P.; Riahi, Z.; Rhim, J.-W. Carrageenan-based functional films integrated with CuO-doped titanium nanotubes for active food-packaging applications. *ACS Sustain. Chem. Eng.* **2021**, *9*, 9300–9307. [CrossRef]
24. Toloman, D.; Pana, O.; Stefan, M.; Popa, A.; Leostean, C.; Macavei, S.; Silipas, D.; Perhaita, L.; Lazar, M.D.; Barbu-Tudoran, L. Photocatalytic activity of SnO_2-TiO_2 composite nanoparticles modified with PVP. *J. Colloid Interface Sci.* **2019**, *542*, 296–307. [CrossRef] [PubMed]
25. Zhang, X.; Li, J.; Wang, X.; Wang, Y.; Hang, R.; Huang, X.; Tang, B.; Chu, P.K. Effects of copper nanoparticles in porous tio2 coatings on bacterial resistance and cytocompatibility of osteoblasts and endothelial cells. *Mater. Sci. Eng. C Mater. Biol. Appl.* **2018**, *82*, 110–120. [CrossRef] [PubMed]

26. Kumar, D.; Saini, N.; Jain, N.; Sareen, R.; Pandit, V. Gold nanoparticles: An era in bionanotechnology. *Expert Opin. Drug Deliv.* **2013**, *10*, 397–409. [CrossRef] [PubMed]
27. Zhang, J.; Mou, L.; Jiang, X. Surface chemistry of gold nanoparticles for health-related applications. *Chem. Sci.* **2020**, *11*, 923–936. [CrossRef]
28. Patil, T.; Gambhir, R.; Vibhute, A.; Tiwari, A.P. Gold nanoparticles: Synthesis methods, functionalization and biological applications. *J. Clust. Sci.* **2022**. [CrossRef]
29. Zhang, X.-D.; Wu, D.; Shen, X.; Liu, P.-X.; Yang, N.; Zhao, B.; Zhang, H.; Sun, Y.-M.; Zhang, L.-A.; Fan, F.-Y. Size-dependent in vivo toxicity of peg-coated gold nanoparticles. *Int. J. Nanomed.* **2011**, *6*, 2071–2081. [CrossRef]
30. Cho, W.-S.; Cho, M.; Jeong, J.; Choi, M.; Cho, H.-Y.; Han, B.S.; Kim, S.H.; Kim, H.O.; Lim, Y.T.; Chung, B.H.; et al. Acute toxicity and pharmacokinetics of 13 nm-sized peg-coated gold nanoparticles. *Toxicol. Appl. Pharmacol.* **2009**, *236*, 16–24. [CrossRef]
31. Zhang, X.-D.; Wu, D.; Shen, X.; Liu, P.-X.; Fan, F.-Y.; Fan, S.-J. In vivo renal clearance, biodistribution, toxicity of gold nanoclusters. *Biomaterials* **2012**, *33*, 4628–4638. [CrossRef]
32. Chen, Y.-S.; Hung, Y.-C.; Liau, I.; Huang, G.S. Assessment of the in vivo toxicity of gold nanoparticles. *Nanoscale Res. Lett.* **2009**, *4*, 858–864. [CrossRef]
33. Devi, L.G.; Kavitha, R. A review on plasmonic metal-TiO_2 composite for generation, trapping, storing and dynamic vectorial transfer of photogenerated electrons across the schottky junction in a photocatalytic system. *Appl. Surf. Sci.* **2016**, *360*, 601–622. [CrossRef]
34. Farrugia, C.; Di Mauro, A.; Lia, F.; Zammit, E.; Rizzo, A.; Privitera, V.; Impellizzeri, G.; Buccheri, M.A.; Rappazzo, G.; Grech, M.; et al. Suitability of different titanium dioxide nanotube morphologies for photocatalytic water treatment. *Nanomaterials* **2021**, *11*, 708. [CrossRef] [PubMed]
35. Wang, T.-T.; Lin, Y.-C.; Lin, M.-C.; Lin, Y.-G. Au-assisted methanol-hydrogenated titanium dioxide for photocatalytic evolution of hydrogen. *Catal. Today* **2020**, *358*, 143–148. [CrossRef]
36. Zhu, H.; Shi, Q.; Lv, W. Study on technique of nanostructured surface of medical titanium prepared by anodic oxidation. *Mater. Sci.* **2013**, *3*, 150–156.
37. Xu, W.; Qi, M.; Li, X.; Liu, X.; Wang, L.; Yu, W.; Liu, M.; Lan, A.; Zhou, Y.; Song, Y. TiO_2 nanotubes modified with au nanoparticles for visible-light enhanced antibacterial and anti-inflammatory capabilities. *J. Electroanal. Chem.* **2019**, *842*, 66–73. [CrossRef]
38. Yu, Y.; Wen, W.; Qian, X.-Y.; Liu, J.-B.; Wu, J.-M. Uv and visible light photocatalytic activity of Au/TiO_2 nanoforests with anatase/rutile phase junctions and controlled au locations. *Sci. Rep.* **2017**, *7*, 41253. [CrossRef]
39. Lishchynskyi, O.; Shymborska, Y.; Stetsyshyn, Y.; Raczkowska, J.; Skirtach, A.G.; Peretiatko, T.; Budkowski, A. Passive antifouling and active self-disinfecting antiviral surfaces. *Chem. Eng. J.* **2022**, *446*, 137048. [CrossRef]
40. Li, Q.; Li, Y.W.; Liu, Z.; Xie, R.; Shang, J.K. Memory antibacterial effect from photoelectron transfer between nanoparticles and visible light photocatalyst. *J. Mater. Chem.* **2010**, *20*, 1068–1072. [CrossRef]
41. Rashid, M.M.; Tomsic, B.; Simoncic, B.; Jerman, I.; Stular, D.; Zorc, M. Sustainable and cost-effective functionalization of textile surfaces with ag-doped TiO_2/polysiloxane hybrid nanocomposite for uv protection, antibacterial and self-cleaning properties. *Appl. Surf. Sci.* **2022**, *595*, 153521. [CrossRef]
42. Liu, Z.; Yin, H.; Liu, H.; Zhang, N.; Zhang, X.; Xu, Q. Antibacterial and photocatalytic degradation properties of TiO_2-based composite. *Int. J. Environ. Anal. Chem.* **2022**. [CrossRef]
43. Liu, L.; Yang, W.; Li, Q.; Gao, S.; Shang, J.K. Synthesis of Cu_2O nanospheres decorated with TiO_2 nanoislands, their enhanced photoactivity and stability under visible light illumination, and their post-illumination catalytic memory. *ACS Appl. Mater. Interfaces* **2014**, *6*, 5629–5639. [CrossRef] [PubMed]
44. Li, J.; Ma, R.; Wu, Z.; He, S.; Chen, Y.; Bai, R.; Wang, J. Visible-light-driven ag-modified TiO_2 thin films anchored on bamboo material with antifungal memory activity against aspergillus niger. *J. Fungi* **2021**, *7*, 592. [CrossRef]
45. Mangram, A.J.; Horan, T.C.; Pearson, M.L.; Silver, L.C.; Jarvis, W.R. Guideline for prevention of surgical site infection, 1999. *Infect. Control Hosp. Epidemiol.* **1999**, *20*, 250–278. [CrossRef]
46. Masters, E.A.; Ricciardi, B.F.; Bentley, K.L.; Moriarty, T.F.; Schwarz, E.M.; Muthukrishnan, G. Skeletal infections: Microbial pathogenesis, immunity and clinical management. *Nat. Rev. Microbiol.* **2022**, *20*, 385–400. [CrossRef]